

## Original Article

**Cite this article:** Saadat S and Stern CR (2023) Genesis of meta-gabbroic crustal xenoliths found in Neogene/Quaternary alkali olivine basalt, northeastern Iran. *Geological Magazine* **160**: 260–273. <https://doi.org/10.1017/S001675682200084X>

Received: 25 October 2021  
Revised: 14 July 2022  
Accepted: 15 July 2022  
First published online: 29 September 2022


**Keywords:**

meta-gabbroic crustal xenoliths; alkali basalts; Ordovician gabbros; NE Iran

**Author for correspondence:**

Saeed Saadat, Email:  
[saeed.saadat@colorado.edu](mailto:saeed.saadat@colorado.edu)

# Genesis of meta-gabbroic crustal xenoliths found in Neogene/Quaternary alkali olivine basalt, northeastern Iran

Saeed Saadat<sup>1</sup>  and Charles R. Stern<sup>2</sup>

<sup>1</sup>Department of Geology and Petroleum Engineering, Mashhad Branch, Islamic Azad University, Mashhad, Iran and

<sup>2</sup>Department of Geological Sciences, University of Colorado, Boulder, CO, USA

**Abstract**

Rounded to angular granoblastic textured mafic xenoliths, ranging from ~1 to 6 cm in dimension, occur together with mantle peridotite xenoliths in a small Neogene/Quaternary alkali basalt cone in northeastern Iran. These crustal xenoliths consist of plagioclase feldspar, clinopyroxene, orthopyroxene and minor olivine, spinel, titanomagnetite and apatite. Their bulk compositions are similar to tholeiitic basalts and they are interpreted as meta-gabbroic rocks derived from mid- to lower crustal depths of 18 to 30 km. Rb–Sr dating suggests an age of  $c. 457 \pm 95$  Ma for these crustal xenoliths, and their geochemistry shows some similarities to Ordovician gabbros that crop out ~20 km to the west. The data suggest that the gabbroic proto-lithologies of the xenoliths formed by intrusion of mafic magmas into the mid- to lower crust, possibly during extension and magmatism related to the opening of the Hercynian Palaeotethys ocean that separated central and eastern Iran from the Eurasian plate during the Late Palaeozoic.

## 1. Introduction

In northeastern Iran (Fig. 1), a small Neogene/Quaternary alkali olivine basalt cone and associate lava flows contain both ultramafic mantle and mafic crustal xenoliths. The chemical and isotopic composition of the basalt and mantle xenoliths were presented in Saadat & Stern (2012) and Su *et al.* (2014), along with mention of, but only very limited petrochemical information for, the mafic crustal xenoliths.

Crustal xenoliths are considered to be fragments of the lower crust accidentally brought to the surface by their host alkali basalts (Rudnick, 1992). Crustal and mantle xenoliths entrained in continental alkali basalts provide samples to study the chemical and physical evolution of the deep continental lithosphere (Selverstone & Stern, 1983; Stern *et al.* 1999; Farmer, 2003; Gautheron *et al.* 2005; Nasir *et al.* 2006); and are the most direct source of information about the composition, age and tectonic history of the lower crust and uppermost mantle lithosphere (Cohen *et al.* 1984; Koornneef *et al.* 2009). The crustal xenoliths found in the alkali basalts of NE Iran are therefore a potentially valuable source of information on the nature of the deeper parts of the crust in this area. This paper presents new major and trace element and isotopic data for these crustal xenoliths as a contribution toward characterizing the lower continental basement below this region.

## 2. Geological overview

The oldest rocks in NE Iran, which are mainly exposed in a narrow elongated NW–SE-trending belt, are Neoproterozoic to Early Palaeozoic (660–530 Ma) in age. These rocks are gneisses and schists, recrystallized limestones and dolomites, and granite and quartz diorite plutons similar to exposures of Neoproterozoic to Early Palaeozoic basement in other tectonic zones of Iran (Hassanzadeh *et al.* 2008). The granites and quartz diorites and rhyolites in NE Iran range in age from 570 to 530 Ma (Bagherzadeh *et al.* 2015; Shafaii Moghadam *et al.* 2017a, b; Oinam *et al.* 2020; Kumar & Pundir, 2021; Samadi *et al.* 2022; Azizi & Whattam 2022). Late Neoproterozoic – Early Palaeozoic mafic and felsic intrusive igneous rocks and associated clastic sediments are also reported from other areas in Iran (Horton *et al.* 2008; Bagherzadeh *et al.* 2015; Shafaii Moghadam *et al.* 2017a, b; Mazhari *et al.* 2019; Sepidbar *et al.* 2020; Azizi & Whattam, 2022), as well as other areas along the northern margin of the Gondwana supercontinent (Hassanzadeh *et al.* 2008; Oinam *et al.* 2020; Kumar & Pundir, 2021; Samadi *et al.* 2022).

Younger gabbros and zircons in the sediments of the Qeli Formation have been dated as 492 to 457 Ma (Fig. 1; Shafaii Moghadam *et al.* 2017a, b; Ranjbar Moghadam *et al.* 2018). It has been suggested that the formation of these gabbroic rocks was a result of an extensional tectonic event

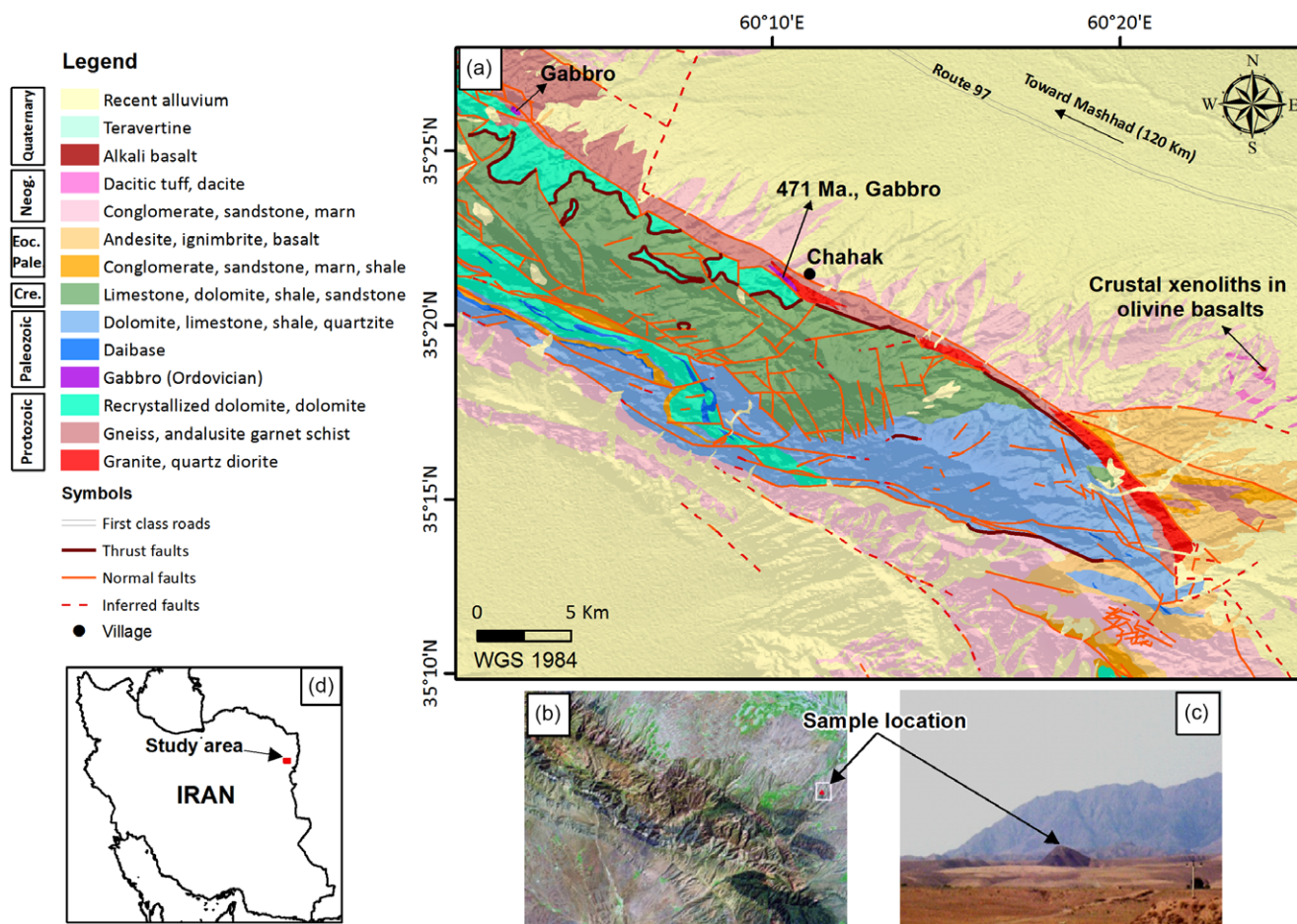


**Fig. 1.** (Colour online) (a) Simplified geological map of the study area in NE Iran showing the location of the outcrop of alkali olivine basalt containing both ultramafic mantle and mafic crustal xenoliths (Saadat & Stern, 2012), as well as the location of Ordovician gabbroic rocks near Chahak ~20 km to the west (Partovifar, 2012; Shojaee kaveh, 2014; Homam, 2015). The base map is taken from Geological Survey of Iran (1984). (b) Satellite image showing the location of the study area. (c) Photo of the outcrop of xenoliths bearing alkali basalt. (d) Location of the study area in NE Iran.

related to the opening of the Palaeotethys ocean during the Ordovician and Silurian (Ranjbar Moghadam *et al.* 2018; Samadi *et al.* 2022).

After this, central and eastern Iran were separated until Late Palaeozoic time from the Eurasian plate by the Hercynian Palaeotethys ocean (Shahabpour, 2005). During the Permian–Triassic, a N-dipping subduction system along the northern Palaeotethys margin led to the closure of this ocean (Golonka, 2004), and the northward motion of the central and eastern Iran micro-continent resulted in their welding with the Eurasian plate (Shahabpour, 2005). The central and eastern Iran – Eurasia collision must have happened at roughly 222–210 Ma (Horton *et al.* 2008). K/Ar analysis of hornblende gabbro remnants of the Palaeotethys oceanic crust, exposed in the Binalud range (Alavi, 1979), correspond to the late Pennsylvanian – early Permian (Ghazi *et al.* 2001). This range extends to the west into the Alborz range and eastward into the Hindu-Kush in northern Iran and Afghanistan.

Mesozoic rocks in this area mainly consist of bedded limestone, dolomite, shale, sandstone and conglomerate, whereas the Palaeogene is marked by volcano-sedimentary rocks. Volcanic rocks are mostly porphyritic basaltic andesites, dacites and rhyodacitic welded tuff (Fig. 1). The latter rocks were dated  $38.5 \pm 1.2$  Ma, indicating a late Eocene – early Oligocene age for the upper

part of the volcano-sedimentary sequence. Neogene sediments, mainly conglomerates and sandstones, form very thick sequences filling in tectonic basins on either side of the main Alborz Mountain range.

The Neogene/Quaternary alkali olivine basalts with ultramafic mantle and mafic crustal xenoliths, which are the focus of this study, consist of a monogenetic basaltic cone and associated lava flows which crop out in a subcircular area of ~60 000 m<sup>2</sup> (0.3 × 0.2 km), overlying unconsolidated Neogene sediments and Tertiary andesitic and dacitic tuffs in NE Iran (Fig. 1; Saadat & Stern, 2012; Su *et al.* 2014). This is the only known occurrence of either mantle or granoblastic textured crustal xenoliths in this area of Iran. Mantle xenoliths are two to three times more abundant than the crustal xenoliths in this basalt flow. The crustal xenoliths are in general 1 to 6 cm in largest dimension, while the ultramafic mantle xenoliths are in some cases as large as 15 cm in largest diameter. These alkali olivine basalts have geochemical affinities with intra-plate oceanic island alkali basalts (OIB) as do other Neogene/Quaternary alkali olivine basalts erupted along the strike-slip faults bounding the Lut block in eastern Iran (Saadat *et al.* 2010). They show no evidence of enrichment of large-ion-lithophile (LIL) relative to high-field strength (HFS) elements as is characteristic of convergent plate boundary magmas that are erupted above subduction zones. In this respect they differ from

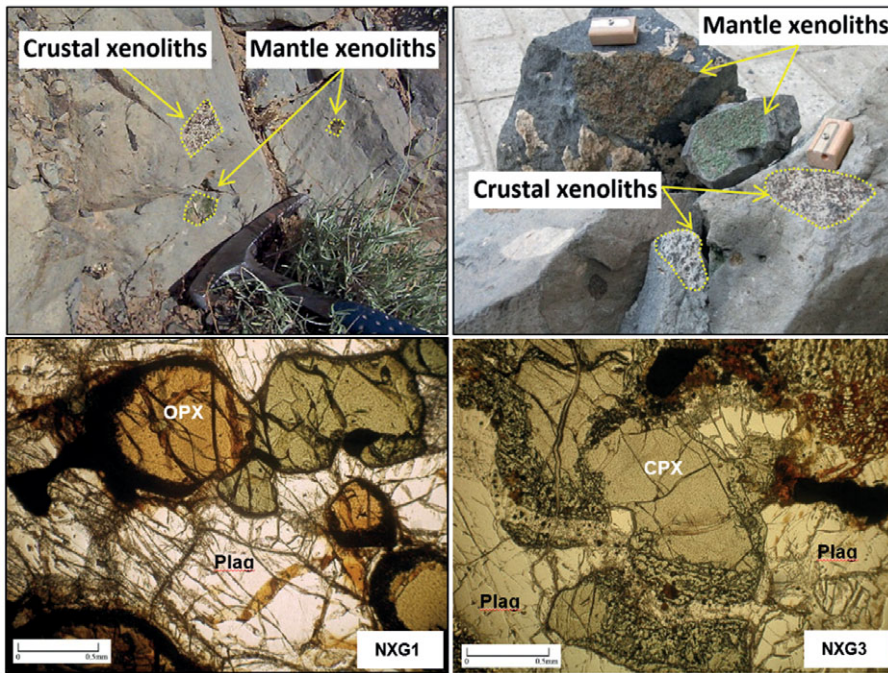


**Fig. 2.** (Colour online) Photos of both crustal and mantle xenoliths in the alkali basalts of NE Iran (Saadat & Stern, 2012) and photomicrographs of a CPX (NXG3) and CPX + OPX (NXG1) gabbroic crustal xenoliths.

the 41 to 2.3 Ma collisional and post-collisional basalt, andesite, adakite and dacite lavas and dikes outcropping >200 km to the NW in the Meshkan area around the large Sar'ahkor composite volcano (Shabanian *et al.* 2012). These have negative HFS element anomalies relative to LIL elements and it has been suggested that their genesis involves melting of a detached slab of oceanic crust foundering after the cessation of subduction, or of mantle previously metasomatized above subducted oceanic crust. In contrast, the genesis of the xenolith-bearing alkali olivine basalts from NE Iran, and other olivine alkali basalts erupted along the strike-slip faults surrounding the Lut block, appears to have been derived from mantle unaffected by subduction-related metasomatism. However, like the magmas erupted or emplaced as dikes in the Meshkan region to the NW, they may have risen through the crust along an area of local extension, such as a pull-apart structure, related to strike-slip faulting (Shabanian *et al.* 2012).

### 3. Methods

Twelve samples of crustal xenoliths were chiselled out of a single lava flow (Fig. 2) associated with the small outcrop of alkali olivine basalt in NE Iran. Polished thin-sections for electron probe microanalysis were prepared from these samples. Minerals were analysed using the JEOL JXA-8230 super probe in the Laboratory for Environmental and Geological Science at University of Colorado–Boulder, with an electron-gun accelerating voltage of 15 kV and a 1  $\mu$ m diameter focused beam. Matrix correction was done by Armstrong's ZAF correction program using natural mineral standards.

Two samples of mafic crustal xenoliths, one two-pyroxene gabbro (SS22) and one clinopyroxene gabbro (SS21), were selected for whole-rock geochemical analysis. A jaw crusher was used to pulverize samples, which were then powdered to 200 mesh in a tungsten carbide shatter box. These powders were sent to Activation Laboratories (Canada), where they were analysed for both major and trace elements.

Pyroxene-rich mafic and plagioclase-rich felsic portions of two crushed two-pyroxene gabbro (SS23 and NXG1) xenoliths were hand-picked for determination of an Rb–Sr age by solid source mass-spectrometry techniques. The mineral separates from these two xenoliths, as well as the bulk whole-rock of xenolith SS23, were analysed for Sr isotopes. Isotopic analyses were done in the isotope lab in the Department of Geological Sciences, University of Colorado. Sample powders for isotopic analysis were generated in a ceramic-lined container.  $^{87}\text{Sr}/^{86}\text{Sr}$  ratios were analysed using a Finnigan-Mat 261 four-collector static mass spectrometer. Replicate analyses of the SRM-987 standard in this mode yielded a mean  $^{87}\text{Sr}/^{86}\text{Sr}$  of  $0.71025 \pm 2$  ( $2\sigma$ ). Measured  $^{87}\text{Sr}/^{86}\text{Sr}$  were corrected to  $\text{SRM-987} = 0.710299 \pm 8$ . Errors are  $2\sigma$  of the mean, which refer to the last two digits of the  $^{87}\text{Sr}/^{86}\text{Sr}$  ratio. Analyses were dynamic mode, three-collector measurements. Details of analytical procedures are given in Farmer *et al.* (1991, 2002).

### 4. Results

#### 4.a. Petrography

The rounded to angular crustal xenoliths are medium-grained granoblastic gabbros (Fig. 2) composed of around 50% plagioclase as well as both clinopyroxene and orthopyroxene and small variable amounts of olivine (<5%), spinel, iron oxides and apatite. Out of the 12 samples collected and thin-sectioned, eight are two-pyroxene gabbros and four are clinopyroxene gabbros without orthopyroxene. Clinopyroxenes have undergone reactions along their borders to produce fine-grained intergrowths of other minerals. Some plagioclases also show spongy texture that could be either original crystallization features or the result of dissolution and/or direct melting caused by heating within the hot mafic host basaltic magma which transported the xenoliths to the surface (Hibbard, 1995). Green spinel, titanomagnetite and apatite are also present in minor amounts. The crustal xenoliths tend to be equigranular, with smooth curving grain boundaries that commonly meet in  $120^\circ$  triple junctions (Fig. 2). Neither garnet, amphibole

nor alkali feldspar has been recognized in any of the xenolith samples.

#### 4.b. Whole-rock geochemistry

The major and trace element compositions for two gabbroic xenoliths, one representative of those containing both clinopyroxene and orthopyroxene (SS22) and another with only clinopyroxene (SS21), are presented in Table 1. For comparison, the average major and trace element concentration are shown for three Ordovician gabbroic rocks which outcrop near Chahak c. 20 km NW of the study area (Figs 1, 3 and 4; Partovifar, 2012; Shojaee kaveh, 2014; Homam, 2015; Ranjbar Moghadam *et al.* 2018).

The two crustal xenoliths have SiO<sub>2</sub> of 45.4 and 52.8 wt %, with moderate MgO contents of 9.5 and 4.9 wt %, and Al<sub>2</sub>O<sub>3</sub> of 15.4 and 17.5 wt %, respectively. Their Cr concentrations range from 370 to 90 ppm (Table 1). These xenoliths plot in the gabbro and gabbro/diorite fields on a silica vs total alkalis classification diagram (Fig. 3). They show metaluminous affinity and plot in the tholeiitic field (Fig. 4; Shand, 1943). Although the two-pyroxene gabbro (SS22) has a major element composition similar to a basalt, the Cpx gabbro (SS21) has lower SiO<sub>2</sub>, Al<sub>2</sub>O<sub>3</sub>, Na<sub>2</sub>O and K<sub>2</sub>O and higher CaO, MgO and Cr, which suggests that this may be a gabbro with enhanced proportions of cumulus clinopyroxene relative to the other mineral phases.

The chondrite-normalized trace-element pattern of the two-pyroxene gabbroic xenolith is characterized by slightly enriched light rare earth elements (LREEs) with La/Yb value of 6.9 (Table 1; Fig. 5). It has only weak negative anomalies of the HFS elements Ti, Hf, Zr, Nb and Th (Fig. 5). The Cpx gabbro has lower La, Sr and Ba, consistent with an increased proportion of clinopyroxene relative to plagioclase in this sample compared to the two-pyroxene gabbro sample, since these elements are either incompatible or less compatible in clinopyroxene relative to Ca-plagioclase (Schnetzler & Philpotts, 1970; Sun, 2018).

#### 4.c. Mineral chemistry

The composition of the plagioclases ranges from An<sub>44-69</sub> and would be classified as labradorite and andesine (Table 2; Fig. 6), whereas the plagioclase phenocrysts in the host basalts include oligoclase as well as andesine and labradorite (Saadat & Stern, 2012).

All clinopyroxenes plot in the augite and diopside fields in the quadrilateral diagram (Table 3; Fig. 6). They have variable Al<sub>2</sub>O<sub>3</sub> and TiO<sub>2</sub> contents (0.5–9.0 wt % and 0.36–1.45 wt %, respectively) and low Cr<sub>2</sub>O<sub>3</sub> <0.86 wt % (Table 3). The Mg# [(Mg<sup>+2</sup>\*100)/((Fe<sup>+2</sup>\*0.85) + (Mg))] for these minerals ranges from 69 to 81. Although clinopyroxenes have a limited composition, they define two groups: first, clinopyroxene from orthopyroxene-free xenoliths, and second, clinopyroxene from two-pyroxene xenoliths. Clinopyroxenes from orthopyroxene-free xenoliths extend to higher Na<sub>2</sub>O and CaO compositions (0.95–1.09 wt % and 19.79–20.23 wt %, respectively) and their Mg# ranges from 72 to 81. Clinopyroxenes from two-pyroxene xenoliths show higher FeO and MgO content and their Mg# ranges from 69 to 78. Clinopyroxenes from this group show lower Na<sub>2</sub>O and CaO content (0.39–0.74 wt % and 17.29–19.82 wt %, respectively). In general, some other notable differences also exist between the compositions of clinopyroxene in these two groups. Al<sub>2</sub>O<sub>3</sub> contents vary from 0.5 to 7.4 wt % in two-pyroxene gabbros, as compared with 8.3 to 8.6 wt % in those with clinopyroxene only (Fig. 7).

**Table 1.** Major oxides (wt %) and trace element (ppm) composition of two crustal xenoliths and Ordovician gabbros from the adjacent Chahak area

Type	CPX	CPX + OPX	Ave.	Ave.	Ave.
	gabbro	gabbro	gabbro	gabbro	gabbro
<b>Sample</b>	SS21	SS22	*	†	‡
SiO <sub>2</sub>	45.6	52.8	50.3	52.0	45.4
TiO <sub>2</sub>	1.1	1.1	1.5	2.5	2.7
Al <sub>2</sub> O <sub>3</sub>	15.4	17.5	13.7	12.2	14.4
FeO	10.6	9.0	10.5	12.6	14.8
MnO	0.2	0.2	0.1	0.3	0.2
MgO	9.5	4.9	7.8	6.4	5.2
CaO	14.5	8.7	9.1	8.3	5.4
Na <sub>2</sub> O	2.1	3.6	2.9	3.1	2.8
K <sub>2</sub> O	0.4	1.7	0.7	0.4	2.4
P <sub>2</sub> O <sub>5</sub>	0.1	0.3	0.1	0.4	0.9
Total	99.5	99.8	96.6	98.2	94.3
K <sub>2</sub> O + Na <sub>2</sub> O	2.5	5.3	3.6	3.5	5.2
N <sub>2</sub> O/K <sub>2</sub> O	5.3	2.1	4.1	7.8	1.2
Cr	370	90			
Cs	0.1	0.1	0.7	23.3	
Rb	21	41	21	25	
Ba	48	325	176	167	
Sr	244	684	323	153	
Nb	3.5	6.9	9.2	5.3	71.4
Ta	0.6	0.7	0.6	0.4	4.8
Zr	62	48	80	121	
Y	29	18	17	32	25
Hf	2.1	1.4	2.3		5.4
Th	0.28	0.37	1.7	2.3	
U	0.08	0.13			1.28
La	3.37	12.8	10.8	11.0	42.3
Ce	10.0	26.5	21.4	31.0	101.2
Pr	1.73	3.41	2.80	4.87	10.5
Nd	9.32	15.0	12.5	23.3	42.3
Sm	3.23	3.62	3.30	7.13	8.33
Eu	1.19	1.25	1.20	2.23	2.54
Gd	4.22	3.78	3.70	9.40	7.41
Tb	0.81	0.59	0.60	1.72	1.20
Dy	5.30	3.34			
Yb	2.90	1.86	1.50	5.90	1.77
Lu	0.44	0.30	0.20	0.87	0.26
La/Nb	1.0	1.9	1.2	2.1	0.6
Ba/Nb	13.7	47.1	19.2	31.3	
La/Yb	1.2	6.9	7.2	1.8	23.8

\*Homam (2015).

†Partovifar (2012).

‡Shojaee kaveh (2014)

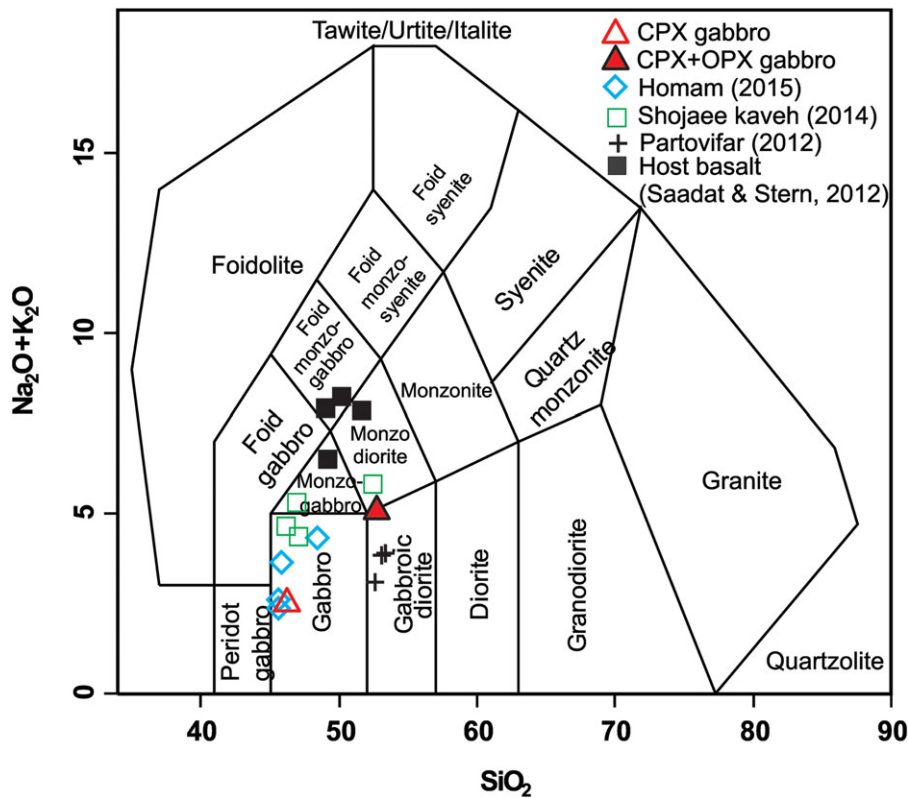


Fig. 3. (Colour online) Petrologic classification, based on Na<sub>2</sub>O + K<sub>2</sub>O (wt %) against SiO<sub>2</sub> (wt %; Middlemost, 1994), for two xenolith samples (triangles) and their host alkali basalt (squares), as well as other mafic rocks from the adjacent Chahak area.

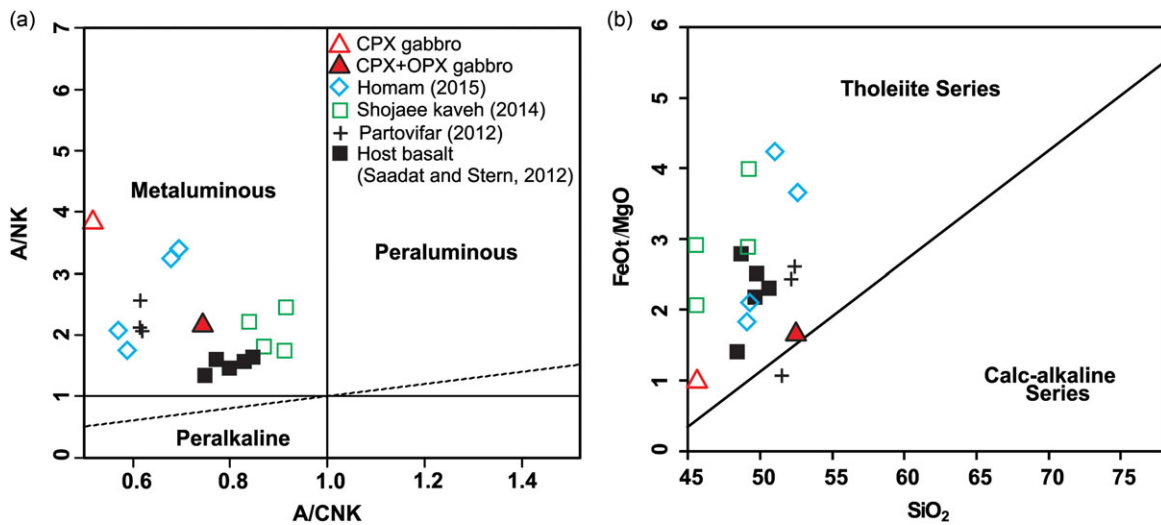


Fig. 4. (Colour online) Plots of various element ratios for crustal xenoliths (triangles) and their host basalt (squares), and other gabbros from NE Iran. In the molecular Al<sub>2</sub>O<sub>3</sub>/Na<sub>2</sub>O + K<sub>2</sub>O vs molecular Al<sub>2</sub>O<sub>3</sub>/CaO + Na<sub>2</sub>O + K<sub>2</sub>O diagram (Maniar & Piccoli, 1989) the xenoliths and other samples classify as metaluminous. In the FeOt/MgO vs SiO<sub>2</sub> diagram (Shand, 1943) they show tholeiitic affinity.

TiO<sub>2</sub> concentrations range from 0.96 to 1.37 wt % in clinopyroxene gabbros compared with 0.36 to 0.88 wt % in two-pyroxene gabbros.

Orthopyroxenes have composition ranges of En<sub>62-69</sub>Fs<sub>29-38</sub>Wo<sub>2-3</sub> and classify as hypersthene (Table 4; Fig. 6). Their Mg# ranges from 65 to 74. Na<sub>2</sub>O and CaO contents are very low (<0.04 wt % and 0.87 to 1.17 wt %, respectively). Olivine in one sample averages Fo63 (Table 5). Spinel has low Cr<sub>2</sub>O<sub>3</sub> (0.51 to 0.67 wt %; Table 6) and belong to the pleonaste solid solution series

(Mg,Fe)Al<sub>2</sub>O<sub>4</sub> between MgAl<sub>2</sub>O<sub>4</sub> (spinel *sensu stricto*) and FeAl<sub>2</sub>O<sub>4</sub> (hercynite).

4.d. Rb-Sr age determination

Rb and Sr concentrations and Sr isotopic ratios of one bulk sample of a two-pyroxene xenolith (SS23) and hand-picked mafic (M; cpx-rich) and felsic (F; feldspar-rich) crushed portions of this same

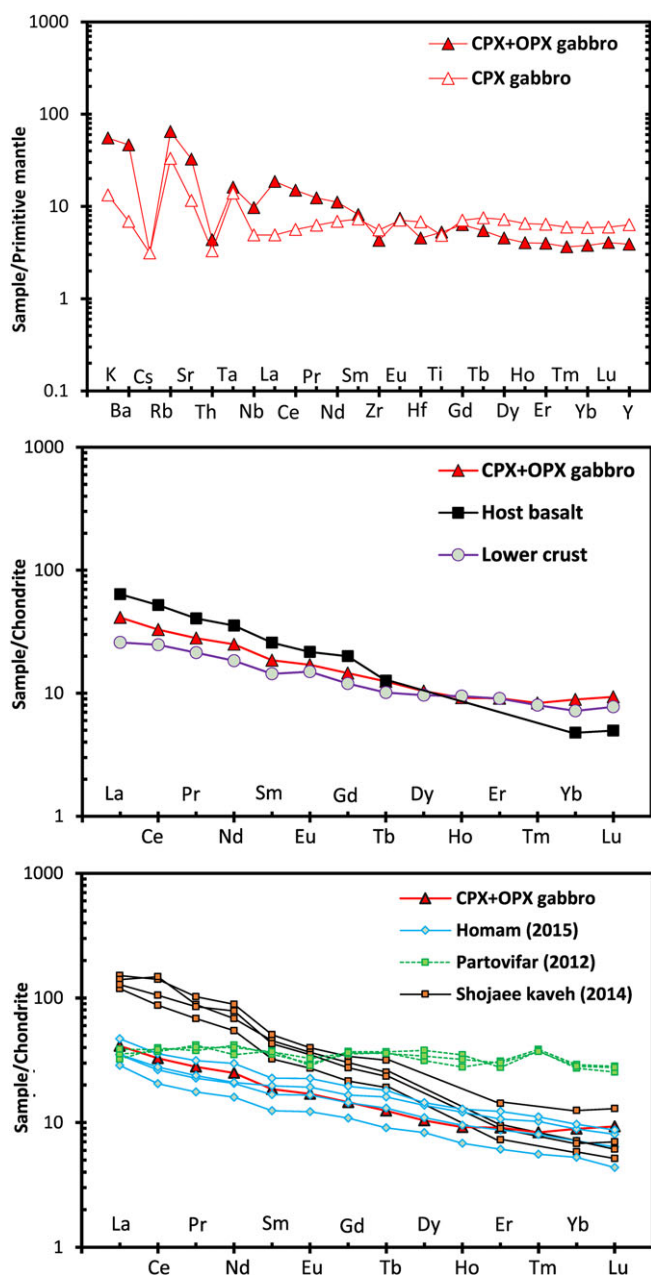


**Fig. 5.** (Colour online) Trace-element compositions of two xenolith samples normalized to (a) primitive mantle and (b, c) a chondritic meteorite and compared to the host basalt (Saadat & Stern, 2012), average lower continental crust (Taylor & McLennan, 1985) and gabbros from adjacent areas in NE Iran (Partovifar, 2012; Shojaee kaveh, 2014; Homam, 2015).

xenolith and of another two-pyroxene xenolith (NXG1) are presented in Table 7. Felsic portions of these samples have significantly higher Sr contents (Table 7). The data plot broadly along a line, suggesting an approximate age of  $457 \pm 95$  Ma (Fig. 8), but both accuracy and precision are low, and this cannot be considered as an isochron.

## 5. Discussion

### 5.a. Xenolith protoliths

The crustal xenoliths from NE Iran are composed of minerals (plagioclase feldspar, clinopyroxene, orthopyroxene, olivine) common

in mafic igneous rock. They lack aluminosilicates (sillimanite, kyanite) common in metasedimentary rocks, and they contain low  $\text{SiO}_2 < 53$  wt % and high  $\text{MgO} > 4.9$  wt %, suggesting an igneous origin. We interpret them as recrystallized gabbros formed originally by crystallization from a mafic magma. We suggest that the two-pyroxene gabbro sample SS22 represents a chilled liquid; a holocrystalline equivalent of an original mafic magma composition, as both its major and trace element chemistry are similar to many basalts. In contrast, Cpx gabbro SS21, with lower  $\text{SiO}_2$ ,  $\text{Na}_2\text{O}$  and  $\text{K}_2\text{O}$ , and higher CaO than most typical basalts, may contain higher proportions of cumulus clinopyroxene. Its unusual convex REE pattern, with middle rare earth elements (MREE) higher than LREE, is also indicative of a Cpx cumulate based on the empirically determined partition coefficients between clinopyroxene and basalt (Schnetzler & Philpotts, 1970; Sun, 2018).

The gabbroic crustal xenoliths are unlikely to be co-genetic with their host alkali basalt. The host basalt plots in the alkali basalt and foidite fields on a total alkali-silica classification diagram (Fig. 3) and in the alkali basalt field of oceanic island basalts (OIB) on trace element discrimination diagrams (Fig. 9), while the gabbroic xenoliths have compositions similar to tholeiitic mid-ocean ridge basalts (MORB). The two-pyroxene xenolith, which we consider to be representative of the basaltic magma from which all the gabbroic xenoliths crystallized, displays trace element contents and REE patterns which are in general very distinct from the host alkali basalt (Fig. 5). For example, Nb and Zr contents in this xenolith are 6.9 and 48 ppm, respectively, significantly lower than the host basalt, with Nb of 46 ppm and Zr of 214 ppm (Saadat & Stern, 2012). The basaltic host rock also has higher  $\text{La/Yb} > 16$  compared to the two-pyroxene gabbroic xenolith with  $\text{La/Yb} < 7$  (Fig. 5). While the basaltic host rocks are Neogene/Quaternary in age, the Sr isotopic data (Fig. 8) suggest, despite the uncertainty in the data, that the xenoliths are significantly older.

The two-pyroxene gabbroic xenolith does not show distinctive negative Nb or Ta anomalies characteristic of subduction-related igneous rocks (Taylor & McLennan, 1985; Kempton *et al.* 1990; Rudnick & Fountain, 1995). This xenolith plots in the tholeiitic MORB field in the Y vs Zr diagram (Fig. 9) and other trace element ratio discrimination diagrams (not shown). The ratios of incompatible trace elements in this xenolith, such as Nb/Yb of 3.7 (Fig. 9), Nb/Th of 18.6 and Ta/U of 5.1, are all similar to MORB.

In summary, the major and trace elements characteristics of the xenoliths classify them as low-K and low-Ti gabbros with tholeiitic MORB affinities and support a MORB-type mantle source for the origin of the tholeiitic basaltic magma from which these gabbroic xenoliths crystallized. Based on its HREE concentrations and the low  $(\text{La/Yb})_N$  of 4.6 and  $\text{Lu/Hf}$  of 0.2, the primary magma from which the two-pyroxene xenolith crystallized can be attributed to melting in the garnet-free spinel facies of MORB-source type upper mantle peridotite (Fig. 10; Frey & Prinz, 1978; Langmuir *et al.* 1992; Thirlwall *et al.* 1994; Beard & Johnson, 1997; Farmer, 2003). This is because, compared with their mantle source, there is only a very small change in La/Yb ratio during spinel-facies melting (Fig. 10), while in contrast, there are large changes in La/Yb associated with melting in the garnet facies (Baker *et al.* 1997).

### 5.b. Thermobarometry

The  $\text{Al}^{\text{IV}}/\text{Al}^{\text{VI}}$  diagram is used to discriminate between pyroxenes from high- and low-pressure origins (Fig. 11; Aoki & Shiba, 1973). Clinopyroxenes from xenoliths show  $\text{Al}^{\text{IV}}/\text{Al}^{\text{VI}}$  ratios ranging from

**Table 2.** Electron probe micro-analysis of plagioclase

Type Sample No.	CPX gabbros				CPX + OPX gabbros						
	SS-21	SS-29	NXM4	NXG3*	SS-23	SS-28	SS-22	NXG1	NXMG2	NXG1*	NXG2*
	1	4	2	1	3	3	3	3	3	1	1
SiO <sub>2</sub>	53.84	54.69	53.63	57.29	55.05	50.27	57.31	55.02	50.33	56.38	57.05
TiO <sub>2</sub>	0.01	0.02	0.01	0.00	0.02	0.01	0.02	0.02	0.01	0.00	0.00
Al <sub>2</sub> O <sub>3</sub>	29.18	28.57	28.43	26.97	29.28	32.41	27.69	27.32	31.52	26.87	26.99
FeO	0.16	0.24	0.15	0.27	0.25	0.28	0.33	0.30	0.25	0.30	0.35
MgO	0.01	0.01	0.02	0.00	0.03	0.02	0.02	0.02	0.01	0.00	0.00
CaO	10.41	9.77	10.03	8.73	10.45	13.86	8.73	8.76	13.16	8.71	8.63
Na <sub>2</sub> O	5.55	3.90	4.37	5.62	4.13	3.31	4.36	4.67	3.53	5.49	5.72
K <sub>2</sub> O	0.17	0.53	0.14	1.21	0.58	0.20	1.15	1.13	0.20	1.19	0.99
Total	99.35	97.74	96.78	100.1	99.80	100.4	99.62	97.25	99.04	98.94	99.72
Number of ions on the basis of 32 oxygens											
Si	9.74	10.19	10.05	10.31	10.03	9.12	10.46	10.25	9.24	10.27	10.3
Al	6.22	6.28	6.28	5.72	6.28	6.92	5.96	6.00	6.82	5.77	5.75
Fe	0.02	0.04	0.02	0.04	0.04	0.04	0.05	0.05	4.96	0.05	0.05
Ca	2.02	1.95	2.01	1.68	2.04	2.69	1.71	1.75	2.59	1.70	1.67
Na	1.95	1.4	1.59	1.96	1.46	1.16	1.54	1.69	1.26	1.94	2.00
K	0.04	0.13	0.04	0.28	0.14	0.05	0.27	0.27	0.05	0.28	0.23
Or	1	4	1	7	4	1	8	7	1	7	6
Ab	49	40	44	50	40	30	44	46	32	50	51
An	50	56	55	43	56	69	48	47	67	44	43

\*Saadat &amp; Stern, 2012.

**Table 3.** Electron probe micro-analysis of clinopyroxenes

Type Sample No.	CPX gabbros			CPX + OPX gabbros					
	SS21	SS29	NXM4	SS22	SS23	SS28	NXMG2	NXG1	NXG1*
	3	3	3	3	3	3	3	2	4
SiO <sub>2</sub>	46.87	45.13	46.41	49.70	48.17	47.62	45.98	47.88	50.40
TiO <sub>2</sub>	1.05	1.37	0.96	0.54	0.77	0.88	1.45	0.69	0.50
Al <sub>2</sub> O <sub>3</sub>	8.58	8.45	8.28	4.41	5.74	7.44	9.02	4.71	3.50
Cr <sub>2</sub> O <sub>3</sub>	0.02	0.02	0.03	0.02	0.06	0.01	0.01	0.01	0.00
FeO	9.60	11.06	9.02	13.27	11.26	10.18	9.92	12.04	10.90
MnO	0.28	0.33	0.26	0.40	0.29	0.35	0.37	0.37	0.30
MgO	11.55	9.42	11.52	12.01	12.22	12.16	11.68	12.25	13.0
CaO	19.84	20.23	19.79	18.76	19.49	19.82	19.41	19.01	18.7
Na <sub>2</sub> O	1.03	1.09	0.95	0.63	0.68	0.73	0.73	0.74	0.60
Total	98.81	97.11	97.22	99.74	98.68	99.19	98.58	97.70	97.90
Cations calculated on the basis of 6 oxygens									
Si	1.79	1.75	1.77	1.88	1.82	1.79	1.74	1.84	1.92
Ti	0.03	0.04	0.03	0.02	0.02	0.03	0.04	0.02	0.02

(Continued)

Table 3. (Continued)

Type	CPX gabbros			CPX + OPX gabbros					
	SS21	SS29	NXM4	SS22	SS23	SS28	NXMG2	NXG1	NXG1*
Sample No.	3	3	3	3	3	3	3	2	4
Al	0.39	0.39	0.37	0.20	0.26	0.33	0.40	0.21	0.16
Fe	0.31	0.43	0.29	0.42	0.36	0.32	0.31	0.39	0.35
Mn	0.01	0.01	0.01	0.01	0.01	0.01	0.01	0.01	0.01
Mg	0.66	0.54	0.66	0.68	0.69	0.68	0.66	0.70	0.74
Ca	0.81	0.84	0.81	0.76	0.79	0.8	0.79	0.78	0.76
Na	0.00	0.08	0.07	0.05	0.05	0.05	0.05	0.05	0.05
En	37	34	40	38	40	40	40	40	40
Wo	46	52	49	42	46	47	47	45	41
Fs	17	14	11	20	15	13	13	15	19
Mg#	72	73	81	69	76	79	78	77	71

\*Saadat & Stern, 2012.

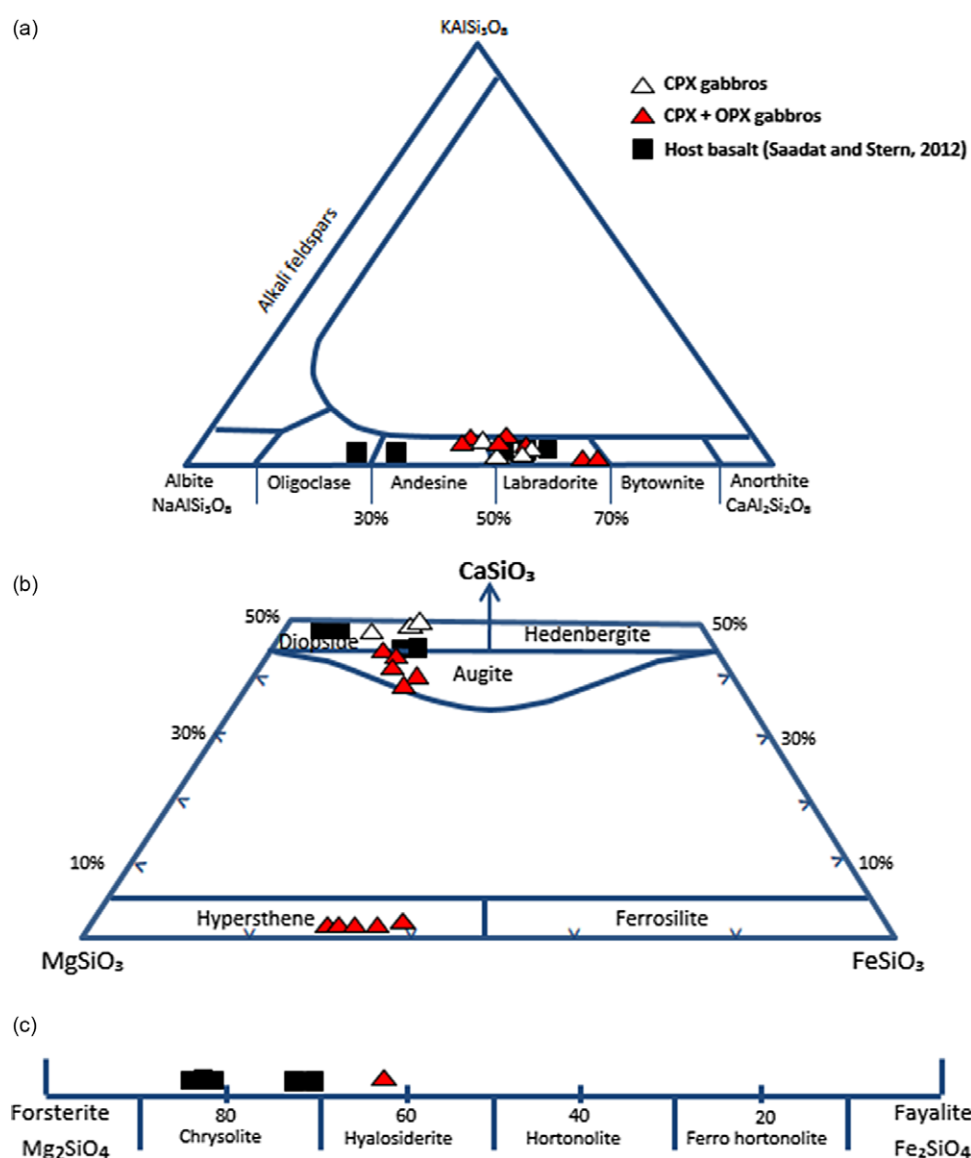
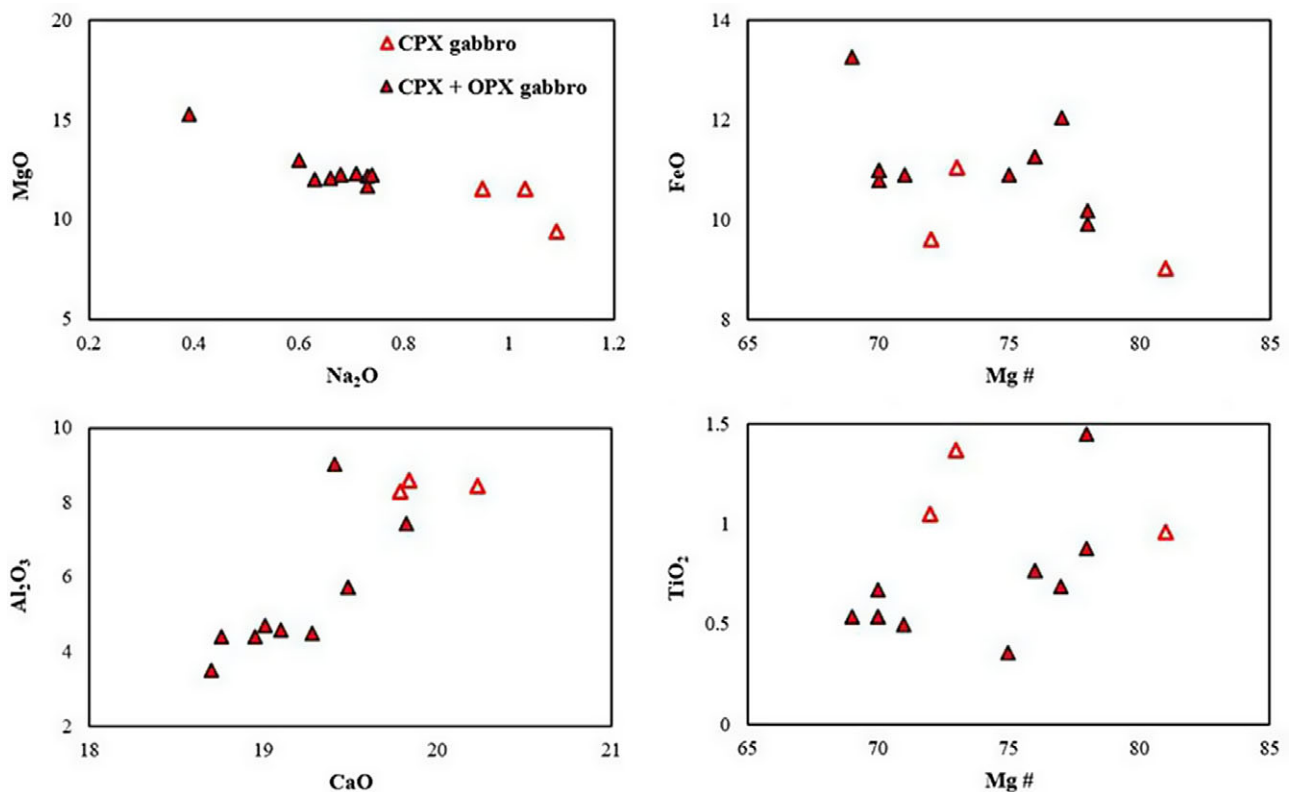


Fig. 6. (Colour online) Compositions of olivines, orthopyroxenes, clinopyroxenes and plagioclases in different crustal xenolith samples compared to their host basalt.



**Table 4.** Electron probe micro-analysis of orthopyroxenes

Type Sample No.	CPX + OPX gabbros					
	SS22 3	SS23 3	SS28 1	NXMG2 3	NGX1 3	NXG1* 3
SiO <sub>2</sub>	50.39	50.10	50.14	48.47	48.86	50.50
TiO <sub>2</sub>	0.20	0.20	0.11	0.29	0.19	0.20
Al <sub>2</sub> O <sub>3</sub>	2.88	3.69	5.28	6.29	3.06	3.10
Cr <sub>2</sub> O <sub>3</sub>	0.02	0.03	0.00	0.00	0.01	0.00
FeO	25.32	22.83	20.30	21.10	22.65	21.6
MnO	0.66	0.53	0.62	0.60	0.60	0.60
MgO	19.89	21.43	23.01	21.96	20.84	20.80
CaO	1.17	1.02	0.87	0.90	1.07	1.10
Na <sub>2</sub> O	0.04	0.04	0.04	0.04	0.04	0.00
Total	100.56	99.88	100.37	99.65	97.32	98.00
Cations calculated on the basis of 6 oxygens						
Si	1.89	1.87	1.84	1.80	1.87	1.92
Ti	0.01	0.00	0.00	0.01	0.01	0.00
Al	0.13	0.16	0.23	0.28	0.14	0.14
Fe	0.79	0.71	0.61	0.67	0.71	0.69
Mn	0.02	0.02	0.02	0.02	0.02	0.02
Mg	1.11	1.19	1.26	1.21	1.19	1.18
Ca	0.05	0.04	0.03	0.04	0.04	0.04
En	60	64	69	68	64	62
Wo	3	2	2	2	2	2
Fs	38	33	29	30	33	36
Mg#	65	69	74	73	69	67

**Fig. 7.** (Colour online) MgO vs Na<sub>2</sub>O, FeO and TiO<sub>2</sub> vs Mg#; and Al<sub>2</sub>O<sub>3</sub> vs TiO<sub>2</sub> in clinopyroxenes from CPX and CPX + OPX gabbroic xenoliths.

**Table 5.** Electron probe micro-analysis of olivine

Type Sample	CPX gabbro		
	NXG 3		
SiO <sub>2</sub>	36.22	36.43	35.98
FeO	31.52	30.71	30.65
MnO	0.81	0.84	0.87
MgO	29.09	30.54	30.97
Total	97.87	98.71	98.65
Cations calculated on the basis of 4 oxygens			
Fe	0.987	0.946	0.943
Mn	0.026	0.026	0.027
Mg	1.623	1.678	1.699
Fo	62	63	64

**Table 6.** Electron probe micro-analysis of spinels

Sample No.	NXM4	SS21
	1	3
SiO <sub>2</sub>	0.00	0.00
TiO <sub>2</sub>	0.23	0.24
Al <sub>2</sub> O <sub>3</sub>	56.31	56.61
Cr <sub>2</sub> O <sub>3</sub>	0.67	0.54
FeO	31.65	33.02
MnO	0.29	0.26
MgO	11.37	10.60
CaO	0.02	0.00
Na <sub>2</sub> O	0.00	0.01
K <sub>2</sub> O	0.00	0.00
Total	100.53	101.28
Cations calculated on the basis of 4 oxygens		
Al	1.80	1.80
Cr	0.01	0.01
Fe	0.72	0.74
Mg	0.46	0.43

**Table 7.** Rb and Sr concentrations and Sr isotopic ratios of bulk and hand-picked mafic (M; cpx-rich) and felsic (F; feldspar-rich) portions of two xenoliths

Sample	Rb	+/-	Sr	+/-	<sup>87</sup> Sr/ <sup>86</sup> Sr	+/-
NXG-1 M	8.9163	0.0008	165.7	0.1	0.705242	0.000011
NXG-1 F	8.8122	0.0007	1022.0	0.4	0.704946	0.000009
SS23 Bulk	38.969	0.0030	659.16	0.05	0.705250	0.000007
SS23 M	20.467	0.0006	169.38	0.04	0.705706	0.000010
SS23 F	28.119	0.0020	1149.6	0.4	0.705108	0.000007

0.66 to 1.2. These ranges indicate that the studied samples were formed in mid- to lower crustal depths rather than in the mantle.

The lack of garnet in the studied xenoliths suggests mid- rather than lower crustal depths of crystallization. A maximum pressure estimate of the studied xenolith samples, based on the mineral assemblages, in particular the absence of garnet, would be *c.* 11 kbar (e.g. Miller, 1982). However, the lack of garnet essentially precludes all high-confidence thermobarometers, which typically involve garnet–pyroxene or garnet–hornblende equilibria. The pyroxene thermobarometer of Putirka *et al.* (2003) and Putirka (2008) gives a crystallizing pressure between 5 and 8 kbar, equivalent to depths of 15–25 km, and a temperature range between 950 and 960 °C using their two-pyroxene geothermometer and

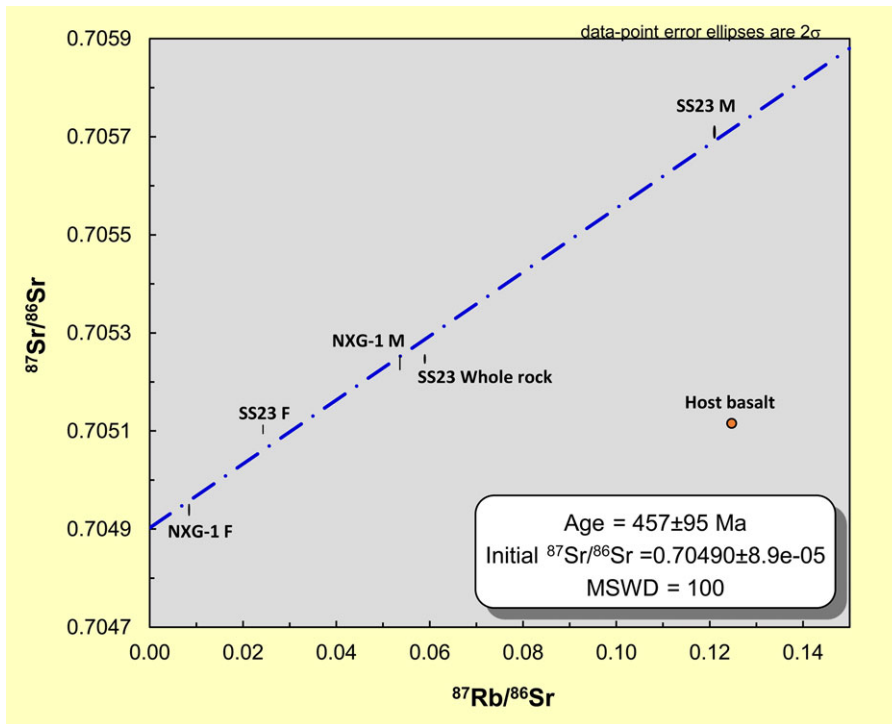


**Fig. 8.** (Colour online) Rb–Sr concentrations and Sr-isotopic data for xenolith samples based on clinopyroxene-rich and plagioclase-rich mafic and felsic separates from two xenolith and one bulk xenolith samples. The  $^{87}\text{Sr}/^{86}\text{Sr}$  and  $^{87}\text{Rb}/^{86}\text{Sr}$  ratio of the host basalts (Saadat & Stern, 2012) is also plotted.

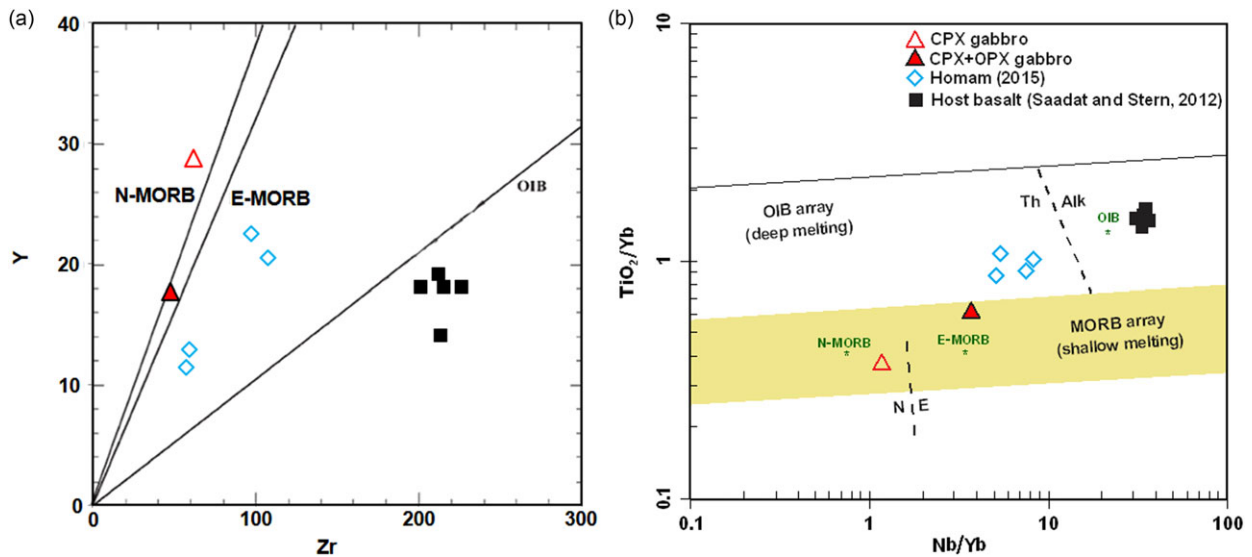


**Fig. 9.** (Colour online) (a) Plot of Y vs Zr (ppm) for crustal xenoliths, their host basalt and gabbros from NE Iran. The xenoliths and gabbros plot in the MORB field. N-MORB (normal), E-MORB (enriched) and OIB are from Sun & McDonough (1989) and Haase *et al.* (1997). (b)  $\text{TiO}_2/\text{Yb}$  vs  $\text{Nb}/\text{Yb}$  (Pearce, 2008) showing the trends for MORB and OIB magmas. The crustal xenoliths are comparable to MORB.

assuming a crystallizing pressure of 6–11 kbar (Fig. 12). In contrast, Su *et al.* (2014) presented equilibrium temperature and pressure estimates of crustal xenoliths from this locality to be *c.* 9 kbar and 850 °C based on an extrapolation of their calculated mantle geotherm into the lower crust (Fig. 12). Mantle xenoliths from the same locality equilibrated in the subcontinental lithosphere at depths of 30 to 60 km and temperatures of 965 °C to 1065 °C (Fig. 12; Saadat & Stern, 2012; Su *et al.* 2014). These estimates

are consistent with a crustal thickness of  $\leq 42$  km below the xenolith locality (Su *et al.* 2014).

**5.c. Regional tectonic implication**

The timing of the intrusion into the crust of the mafic magmas that crystallized to form the gabbroic proto-lithologies of the meta-gabbroic crustal xenoliths from NE Iran is uncertain, but the Sr

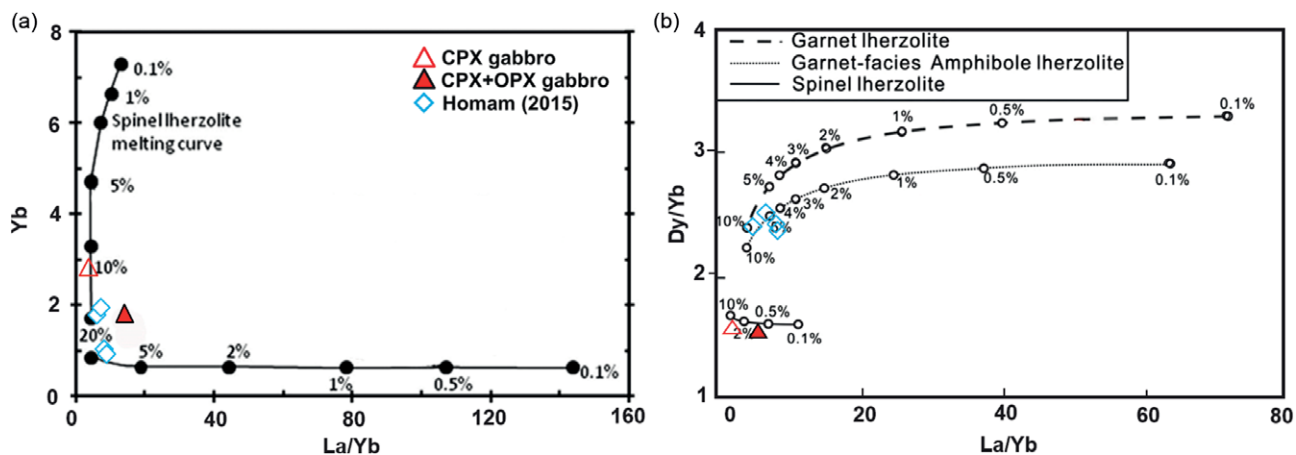


**Fig. 10.** (Colour online) (a) Yb vs La/Yb, and (b) Dy/Yb vs La/Yb, for the xenolith and nearby gabbros, compared to fractional melting curves for spinel (0.578 Ol, 0.270 Opx, 0.119 Cpx and 0.033 Sp that melts in the proportions 0.10 Ol, 0.27 Opx, 0.50 Cpx and 0.13 Sp) and garnet (0.598 Ol, 0.211 Opx, 0.076 Cpx and 0.115 Gt that melts in the proportions 0.05 Ol, 0.20 Opx, 0.30 Cpx and 0.45 Gt) lherzolites.

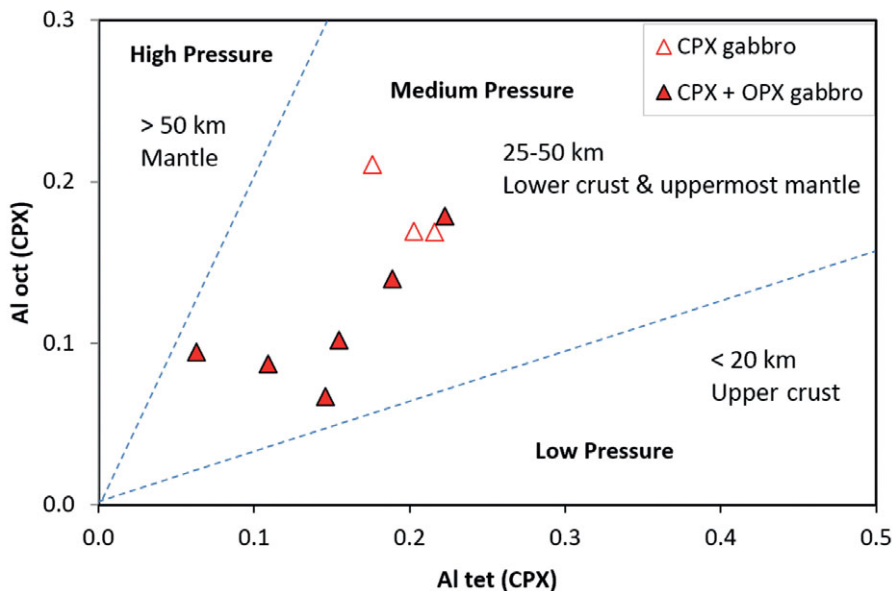


**Fig. 11.** (Colour online) Al<sup>IV</sup> vs Al<sup>VI</sup> diagram for clinopyroxenes. Pressure domains are from Aoki & Shiba (1973).

isotopic data suggest a possible Ordovician age (Fig. 8). Ordovician mafic magmatism in NE Iran is represented by some exposures of Ordovician gabbros in the Chahak area (Fig. 1; Partovifar, 2012; Shojaee kavah, 2014; Homam, 2015) ~20 km NW of the Neogene/Quaternary alkali basalts that contain the meta-gabbroic xenoliths described above. It has been suggested that the formation of these mafic Ordovician igneous rocks, covered by weakly or unmetamorphosed Ordovician sediments with zircon age peaks of 450–492 Ma (Stampfli *et al.* 1991; Stampfli & Borel, 2002; Shafaii Moghadam *et al.* 2017a, b), was the result of a short orogenic event related to the opening of the Palaeotethys ocean during the Ordovician and Silurian (Ranjbar Moghadam *et al.* 2018).

The major and trace element concentration in the meta-gabbroic crustal xenoliths are similar to the Ordovician age tholeiitic hornblende gabbros from the Chahak area (Table 1; Figs 3, 4 and 5). The tholeiitic geochemistry of both the meta-gabbroic crustal xenoliths and these Ordovician gabbros is

consistent with an origin by shallow spinel–lherzolite mantle melting of a MORB-source type mantle, possibly related to rifting associated with the formation of the Palaeotethys ocean basin. However, more work is needed to obtain a precise age for the intrusion of the mafic magmas that formed the proto-lithology of the meta-gabbroic crustal xenoliths.

### 6. Conclusions

- 1) The crustal xenoliths hosted within Neogene/Quaternary alkali basalt in NE Iran rose to the surface rapidly in magmas erupted along pathways associated with local extension produced by NE–SW-trending strike-slip faults (Saadat & Stern, 2012).
- 2) The xenoliths are classified as meta-gabbros with tholeiitic affinities. Geothermobarometry indicates these xenoliths recrystallized at middle to lower crustal conditions.

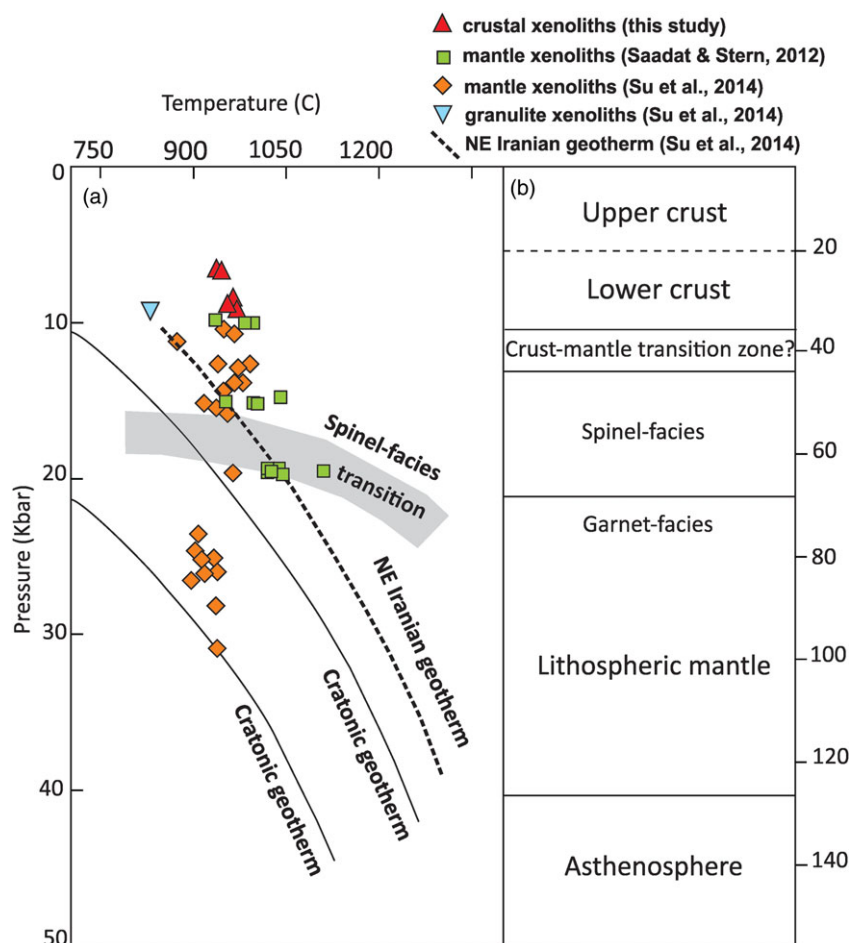


**Fig. 12.** (Colour online) The crustal and upper mantle structure below NE Iran, modified from Su *et al.* (2014) based on the pressure and temperature conditions of equilibrium of the mafic crustal and ultramafic mantle xenoliths.

- 3) The tholeiitic mafic magmas from which the gabbroic xenoliths crystallized were produced by moderate degrees of partial melting of a MORB-source type spinel-lherzolite mantle, possibly as a result of Ordovician magmatic activity related to the opening of the Palaeotethys ocean.

**Acknowledgements.** We would like to thank Lang Farmer and Emily Verplanck for granting us access to their thermal ionization mass-spectrometry (TIMS) laboratory and their assistance in obtaining the isotopic data for this study. We are grateful to Dr Ghoorchi for her support in preparing figures, and H Ebrahimzadeh and H Maadani for their assistance in the field. We also want to thank H Downes and two anonymous reviewers, as well as the editors KM Goodenough and S Sherlock, for constructive comments that improved the final manuscript.

## References

- Alavi M (1979) The Virani ophiolite complex and surrounding rocks. *Geologische Rundschau* **68**, 334–41.
- Aoki KI and Shiba I (1973) Pyroxenes from lherzolite inclusions of Itinome-Gata, Japan. *Lithos* **6**, 41–51.
- Azizi H and Whattam SA (2022) Does Neoproterozoic-Early Paleozoic (570–530 Ma) basement of Iran belong to the Cadomian Orogeny? *Precambrian Research* **368**, 106474.
- Bagherzadeh RM, Karimpour MH, Farmer GL, Stern CR, Santos JF, Rahimi B and Heidarian Shahri MR (2015) U–Pb zircon geochronology, petrochemical and Sr–Nd isotopic characteristic of late Neoproterozoic granitoid of the Bornaward complex (Bardaskan-NE Iran). *Journal of Asian Earth Sciences* **111**, 54–71.
- Baker JA, Menzies MA, Thirlwall MF and MacPherson CG (1997) Petrogenesis of Quaternary intraplate volcanism, Sana'a, Yemen: implications for plume–lithosphere interaction and polybaric melt hybridization. *Journal of Petrology* **38**, 1359–90.
- Beard BL and Johnson CM (1997) Hafnium isotope evidence for the origin of Cenozoic basaltic lavas from the southwestern United States. *Journal of Geophysical Research* **102**, 20149–78.
- Cohen RS, O'Nions RK and Dawson JB (1984) Isotope geochemistry of xenoliths from East Africa: implications for development of mantle reservoirs and their interaction. *Earth and Planetary Science Letters* **68**, 209–20.
- Farmer GL (2003) Continental basaltic rocks. *Treatise on Geochemistry* **3**, 1–39.
- Farmer GL, Broxton DE, Warren RG and Pickthorn W (1991) Nd, Sr, and O isotopic variations in metaluminous ash-flow tuffs and related volcanic rocks at the Timber Mountain/Oasis Valley Caldera, Complex, SW Nevada: implications for the origin and evolution of large-volume silicic magma bodies. *Contributions to Mineralogy and Petrology* **109**, 53–68.
- Farmer GL, Glazner AF and Manley CR (2002) Did lithospheric delamination trigger late Cenozoic potassic volcanism in the southern Sierra Nevada, California? *Geological Society of America Bulletin* **114**, 754–68.
- Frey FA and Prinz M (1978) Ultramafic inclusions from San Carlos, Arizona: petrologic and geochemical data bearing on their petrogenesis. *Earth and Planetary Science Letters* **38**, 129–76.
- Gautheron C, Moreira M and Allègre C (2005) He, Ne and Ar composition of the European lithospheric mantle. *Chemical Geology* **217**, 97–112.
- Geological Survey of Iran (GSI) (1984) *Kariz-Now*, Geological Map, 1:100000. Tehran: Geological Survey of Iran.
- Ghazi AM, Hassanipak AA, Tucker PJ, Mobasher K and Duncan RA (2001) Geochemistry and  $^{40}\text{Ar}$ – $^{39}\text{Ar}$  ages of the Mashhad Ophiolite, NE Iran: a rare occurrence of a 300 Ma (Paleo-Tethys) oceanic crust. *AGU Fall Meeting Abstracts*, V12C-0993.

- Golonka J** (2004) Plate tectonic evolution of the southern margin of Eurasia in the Mesozoic and Cenozoic. *Tectonophysics* **381**, 235–73.
- Haase KM, Stoffers P and Garbe-Schönberg CD** (1997) The petrogenetic evolution of lavas from Easter Island and neighboring seamounts, near-ridge hotspot volcanoes in the SE Pacific. *Journal of Petrology* **38**, 785–813.
- Hassanzadeh J, Stockli DF, Horton BK, Axen GJ, Stockli LD, Grove M, Schmitt AK and Walker JD** (2008) U-Pb zircon geochronology of late Neoproterozoic–Early Cambrian granitoids in Iran: implications for paleogeography, magmatism, and exhumation history of Iranian basement. *Tectonophysics* **451**, 71–96.
- Hibbard MJ** (1995) *Petrography to Petrogenesis*. New Jersey: Prentice-Hall, Inc, 587 pp.
- Homam S** (2015) Petrology and geochemistry of Late Proterozoic hornblende gabbros from southeast of Fariman, Khorasan Razavi province, Iran. *Journal of Economic Geology* **7**, 91–109.
- Horton BK, Hassanzadeh J, Stockli DF, Axen GJ, Gillis RJ, Guest B, Amini AH, Fakhari M, Zamanzadeh SM and Grove M** (2008) Detrital zircon provenance of Neoproterozoic to Cenozoic deposits in Iran: implications for chronostratigraphy and collisional tectonics. *Tectonophysics* **451**, 97–122.
- Kempton PD, Harmon RS, Hawkesworth CJ and Moorbath S** (1990) Petrology and geochemistry of lower crustal granulites from the Geronimo Volcanic Field, southeastern Arizona. *Geochimica et Cosmochimica Acta* **54**, 3401–26.
- Koornneef JM, Davies GR, Döpp SP, Vukmanovic Z, Nikogosian IK and Mason PR** (2009) Nature and timing of multiple metasomatic events in the sub-cratonic lithosphere beneath Labait, Tanzania. *Lithos* **112**, 896–912.
- Kumar S and Pundir S** (2021) Tectono-magmatic evolution of granitoids in the Himalaya and Trans-Himalaya. *Himalayan Geology* **42**, 213–46.
- Langmuir CH, Klein EM and Plank T** (1992) Petrological systematics of mid-ocean ridge basalts: constraints on melt generation beneath ocean ridges. *Geophysical Monograph* **71**, 183–280.
- Maniar PD and Piccoli PM** (1989) Tectonic discrimination of granitoids. *Geological Society of America Bulletin* **101**, 635–43.
- Mazhari SA, Klötzli U and Safari M** (2019) U-Pb geochronology, petrogenesis and tectonomagmatic evolution of uppermost Neoproterozoic-lower Cambrian intrusive rocks in Kaboodan area, NE of Iran. *International Geology Review* **62**, 1971–87.
- Middlemost EAK** (1994) Naming materials in the magma/igneous rock system. *Earth Science Reviews* **37**, 215–24.
- Miller C** (1982) Geochemical constraints on the origin of xenolith-bearing alkali basaltic rocks and megacryst from the Hoggar, central Sahara. *Geochemical Journal* **16**, 225–36.
- Nasir S, Al-Sayigh A, Alharthy A and Al-Lazki A** (2006) Geochemistry and petrology of Tertiary volcanic rocks and related ultramafic xenoliths from the central and eastern Oman Mountains. *Lithos* **90**, 249–70.
- Oinam G, Singh AK, Joshi M, Dutt A, Singh MR, Singh NL and Singh RB** (2020) Continental extension of northern Gondwana margin in the Eastern Himalaya: constraints from geochemistry and U–Pb zircon ages of mafic intrusives in the Siang window, Arunachal Himalaya, India. *Comptes Rendus Geoscience* **352**, 19–41.
- Partovifar F** (2012) *The petrology and geochemical studies of granitic rocks, of Chahak village, Kariz-Now area (southeast of Fariman, Khorassan-e-Razavi), Iran*. MS thesis, Ferdowsi University of Mashhad, Mashhad, Iran (in Persian with English summary).
- Pearce JA** (2008) Geochemical fingerprinting of oceanic basalts with applications to ophiolite classification and the search for Archean oceanic crust. *Lithos* **100**, 14–48.
- Putirka KD** (2008) Thermometers and barometers for volcanic systems. *Reviews in Mineralogy and Geochemistry* **69**, 61–120.
- Putirka KD, Mikaelian H, Ryerson F and Shaw H** (2003) New clinopyroxene-liquid thermobarometers for mafic, evolved, and volatile-bearing lava compositions, with applications to lavas from Tibet and the Snake River Plain, Idaho. *American Mineralogist* **88**, 1542–54.
- Ranjbar Moghadam F, Masoudi F, Homam M, Kerfo F and Mohajel M** (2018) Introducing Ordovician plutonism as a result of Caledonian orogeny from North East of Iran. *Iranian Journal of Crystallography and Mineralogy* **25**, 871–8 (in Persian with English summary).
- Rudnick RL** (1992) Xenoliths – samples of the lower continental crust. In *Continental Lower Crust* (eds DM Fountain, R Arculus and RW Kay), pp. 269–316. Amsterdam: Elsevier.
- Rudnick RL and Fountain DM** (1995) Nature and composition of the continental crust: a lower crustal perspective. *Reviews of Geophysics* **33**, 267–309.
- Saadat S, Karimpour MH and Stern CR** (2010) Petrochemical characteristics of Neogene and Quaternary alkali olivine basalts from the western margin of the Lut block, eastern Iran. *Iranian Journal of Earth Sciences* **2**, 87–106.
- Saadat S and Stern CR** (2012) Petrochemistry of a xenolith-bearing Neogene alkali olivine basalt from northeastern Iran. *Journal of Volcanology and Geothermal Research* **225–226**, 13–29.
- Samadi R, Torabi G, Dantas EL, Morishita T and Kawabata H** (2022) Ordovician crustal thickening and syn-collisional magmatism of Iran: Gondwana basement along the north of the Yazd Block (Central Iran). *International Geology Review* **64**, 2151–65.
- Schnetzer CC and Philpotts JA** (1970) Partition coefficients of rare-earth elements between igneous matrix material and rock-forming mineral phenocrysts-II. *Geochimica et Cosmochimica Acta* **34**, 331–40.
- Selverstone J and Stern CR** (1983) Petrochemistry and recrystallization history of granulite xenoliths from the Pali-Aike volcanic field, Chile. *American Mineralogist* **68**, 1102–12.
- Sepidbar F, Moghadam HS, Li C, Stern RJ, Jiantang P and Vesali Y** (2020) Cadomian magmatic rocks from Zarand (SE Iran) formed in a retro-arc basin. *Lithos* **366**, 105569.
- Shabaniyan E, Acocella V, Gioncada A, Ghasemi H and Bellier O** (2012) Structural control on volcanism in intraplate post collisional settings: Late Cenozoic to Quaternary examples of Iran and Eastern Turkey. *Tectonics* **31**. doi: [10.1029/2011TC003042](https://doi.org/10.1029/2011TC003042).
- Shafaii Moghadam H, Li XH, Griffin WL, Stern RJ, Thomsen TB, Meinhold G, Aharipour R and O'Reilly SY** (2017a) Early Paleozoic tectonic reconstruction of Iran: tales from detrital zircon geochronology. *Lithos* **268–271**, 87–101.
- Shafaii Moghadam H, Li XH, Santos JF, Stern RJ, Griffin WL, Ghorbani G and Sarebani N** (2017b) Neoproterozoic magmatic flare-up along the N. margin of Gondwana: the Taknar complex, NE Iran. *Earth and Planetary Science Letters* **474**, 83–96.
- Shahabpour J** (2005) Tectonic evolution of the orogenic belt in the region located between Kerman and Neyriz. *Asian Earth Sciences* **24**, 405–17.
- Shand SJ** (1943) *The Eruptive Rocks*. New York: John Wiley, 444 pp.
- Shojaee kaveh N** (2014) *Petrology and geochemistry of granitoid rocks in the north and northwest of Torbat-e Jam (Northeast of Iran)*. MS thesis, Ferdowsi University of Mashhad, Mashhad, Iran (in Persian with English summary).
- Stampfli GM and Borel GD** (2002) A plate tectonic model for the Paleozoic and Mesozoic constrained by dynamic plate boundaries and restored synthetic oceanic isochrons. *Earth and Planetary Science Letters* **196**, 17–33.
- Stampfli GM, Marcoux J and Baud A** (1991) Tethyan margins in space and time. *Palaeogeography, Palaeoclimatology, Palaeoecology* **87**, 373–409.
- Stern CR, Kilian R, Olker B, Hauri EH and Kyser TK** (1999) Evidence from mantle xenoliths for relatively thin (~100 km) continental lithosphere below the Phanerozoic crust of southernmost South America. *Lithos* **48**, 217–35.
- Su BX, Chung SL, Zarrinkoub MH, Pang KN, Chen L, Ji WQ, Brewer A, Ying JF and Khatib MM** (2014) Composition and structure of the lithospheric mantle beneath NE Iran: constraints from mantle xenoliths. *Lithos* **202**, 267–82.
- Sun C** (2018) Partitioning and partition coefficients. In *Encyclopedia of Geochemistry* (ed WM White), pp. 1186–97. Encyclopedia of Earth Sciences Series. Dordrecht: Springer. [https://doi.org/10.1007/978-3-319-39312-4\\_347](https://doi.org/10.1007/978-3-319-39312-4_347).
- Sun SS and McDonough MF** (1989). Chemical and isotopic systematics of oceanic basalts: implications for mantle composition and processes. In *Magmatism in the Ocean Basins* (eds AD Saunders and MJ Norry), pp. 313–45. Geological Society of London, Special Publication no. 42.
- Taylor SR and McLennan SM** (1985) *The Continental Crust: Its Composition and Evolution*. Oxford: Blackwell Scientific Publications, 312 pp.
- Thirlwall MF, Upton BG and Jenkins C** (1994) Interaction between continental lithosphere and the Iceland plume Sr–Nd–Pb isotope geochemistry of Tertiary basalts, NE Greenland. *Journal of Petrology* **35**, 839–79.